Journal of Non-Crystalline Solids

Structure of binary antimony phosphate glasses by diffraction methods

--Manuscript Draft--

Manuscript Number:	NOC-D-22-00018
Article Type:	Full Length Article
Keywords:	glass structure, steric effects of lone-pairs, phosphate glass, neutron diffraction, X-ray diffraction
Corresponding Author:	Uwe Hoppe, Ph.D. Rostock University Rostock, GERMANY
First Author:	Uwe Hoppe, Ph.D.
Order of Authors:	Uwe Hoppe, Ph.D.
	Andreas Schöps, Ph.D.
	Alex C. Hannon, Ph.D.
	Andrea Barz, Ph.D.
	Dörte Stachel, Ph.D.
Abstract:	Antimony phosphate glasses (Sb2O3)x(P2O5)1-x with x = 0.05 and 0.80 were measured by neutron and X-ray diffraction with high real-space resolution. The P−O and O−O distance peaks of the PO4 tetrahedra were found with the expected parameters. For the glass of x = 0.80 the Sb−O and O−O coordination numbers and distances suggest strongly distorted SbO3 and SbO4 pyramids according to the lone-pair effects of the Sb3+. The fraction of SbO4 has the right portion that all oxygens can form Sb−O−Sb or Sb−O−P bridges. The first diffraction peak at 13 nm-1 is related to distances between stacked layers of corner-connected oxygen triangles as in orthorhombic Sb2O3. For the glass of x = 0.05 the medium-range order reminds that of vitreous P2O5. The SbO4 units are formed with mean Sb−O bonds of 0.210 nm. Sb2O3 reveals as a good network-forming oxide, better than Sb2O5.
Suggested Reviewers:	Diane Holland, PhD University of Warwick Department of Physics d.holland@warwick.ac.uk excellent knowledge of oxide glasses, lone-pair effects, NMR
	Emma Barney, PhD Assistent professor, University of Nottingham emma.barney@nottingham.ac.uk excellent experticein oxide glasses, diffraction methods
	Hellmut Eckert, PhD Professor, Westfälische Wilhelms-Universität Münster: Westfalische Wilhelms-Universitat Munster eckerth@uni-muenster.de excellent expertice in NMR methods, structure of various oxide glasses, co-author of an earlier paper on Sb phosphate glasses

Dr. Uwe Hoppe
Institut für Physik
Universität Rostock
Albert-Einstein-Straße 23
18051 Rostock Germany

To the Editor
J. Non-Crystalline Solids (ELSEVIER)

Dear Sir, Rostock, 4 Jan 2022

the manuscript “Structure of binary antimony phosphate glasses by diffraction methods” is submitted for publication in J. Non-Cryst. Solids (subscription part).

Results for only two samples are available. Nevertheless, diffraction results on antimony phosphate glasses have never been reported before.

There is only one single file (Word 2016) with all tables, figures etc. in this first submission. The manuscript has never been sent before anywhere else.

Yours sincerely
Uwe Hoppe (corresponding author)

List of possible reviewers:

Prof. Dr. Hellmut Eckert, Westfälische Wilhelms-Universität Münster, Inst. für Physikalische Chemie Münster, Germany
eckerth@uni-muenster.de
Dr. Diane Holland, University of Warwick, Dept. Physics, Coventry, UK
d.holland@warwick.ac.uk
Prof. Dr. Emma Barney, University of Nottingham, Faculty of Engineering, Nottingham, UK
Emma.barney@nottingham.ac.uk
Prof. Dr. Lionel Montagne, Université de Lille, Faculte des Sciences et Technologies, Dept. Chimie, Lille, France
Lionel.montagne@univ-lille.fr

Funding:
This research did not receive any specific grant from funding agencies in the public, commercial, or not-for-profit sectors.

Concerning the authorship I send this list of contributions.

CRediT author statement:
Uwe Hoppe: Conceptualization, Investigation, Formal analysis, Writing – original draft. Andreas Schöps: Resources, Investigation. Alex Hannon: Resources, Investigation, Software. Andrea Barz: Resources, Investigation. Dörte Stachel: Conceptualization, Resources, Writing – Review and Editing.

Manuscript of “Structure of binary antimony phosphate glasses by diffraction methods”

Concerning the authorship I give this list of contributions of the different authors.

CRediT author statement:
Uwe Hoppe: Conceptualization, Investigation, Formal analysis, Writing – original draft.
Andreas Schöps: Resources, Investigation.
Alex Hannon: Resources, Investigation, Software.
Andrea Barz: Resources, Investigation.
Dörte Stachel: Conceptualization, Resources, Writing – Review and Editing.

Abstract

Antimony phosphate glasses $(Sb_2O_3)_x(P_2O_5)_{1-x}$ with x = 0.05 and 0.80 were measured by neutron and X-ray diffraction with high real-space resolution. The P−O and O−O distance peaks of the PO_4 tetrahedra were found with the expected parameters. For the glass of x = 0.80 the Sb−O and O−O coordination numbers and distances suggest strongly distorted SbO_3 and SbO_4 pyramids according to the lone-pair effects of the Sb^{3+}. The fraction of SbO_4 has the right portion that all oxygens can form Sb−O−Sb or Sb−O−P bridges. The first diffraction peak at 13 nm^{-1} is related to distances between stacked layers of corner-connected oxygen triangles as in orthorhombic Sb_2O_3. For the glass of x = 0.05 the medium-range order reminds that of vitreous P_2O_5. The SbO_4 units are formed with mean Sb−O bonds of 0.210 nm. Sb_2O_3 reveals as a good network-forming oxide, better than Sb_2O_5.

Structure of binary antimony phosphate glasses by diffraction methods

U. Hoppe[a*], A. Schöps[b], A. C. Hannon[c], A. Barz[d,e], D. Stachel[d]

[a] Institut für Physik, Universität Rostock, Rostock 18051, Germany

[b] DESY Photon Science, Notkestraße 85, Hamburg 22607, Germany

[c] ISIS facility, Rutherford Appleton Laboratory, Chilton, Didcot, Oxon OX11 0QX, UK

[d] Otto-Schott-Institut für Materialforschung, Friedrich-Schiller-Universität Jena, Fraunhoferstraße 6, Jena 07743, Germany

[e] present address: Fachbereich Sci Tec, Ernst-Abbe-Hochschule Jena, Jena 07745, Germany

* Corresponding author: U. Hoppe uwe.hoppe@uni-rostock.de.

(Highlights)

(1) Glasses $(Sb_2O_3)_x(P_2O_5)_{1-x}$ are obtained in the full range of x except for ~0.5 and $x \rightarrow 1.0$.

(2) Three-fold linked SbO_3 or PO_4 dominate the networks of the Sb_2O_3- or P_2O_5-rich glasses.

(3) The double peaks in the low-Q ranges of the scattering data suggest a stacking of layers.

(4) The SbO_4 dominate in the P_2O_5-rich glasses though sufficient O ligands would allow SbO_6.

(5) Strong lone-pair effects of Sb^{3+} cause short O−O edges (0.28 nm) of the SbO_3-/SbO_4-units.

(Keywords)

glass structure, lone-pair effects, phosphate glass, X-ray diffraction, neutron diffraction

(Abstract)

Antimony phosphate glasses $(Sb_2O_3)_x(P_2O_5)_{1-x}$ with x = 0.05 and 0.80 were measured by neutron and X-ray diffraction with high real-space resolution. The P−O and O−O distance peaks of the PO_4 tetrahedra were found with the expected parameters. For the glass of x = 0.80 the Sb−O and O−O coordination numbers and distances suggest strongly distorted SbO_3 and SbO_4 pyramids according to the lone-pair effects of the Sb^{3+}. The fraction of SbO_4 has the right portion that all oxygens can form Sb−O−Sb or Sb−O−P bridges. The first diffraction peak at 13 nm^{-1} is related to distances between stacked layers of corner-connected oxygen triangles as in the orthorhombic Sb_2O_3. For the glass of x = 0.05 the medium-range order reminds that of vitreous P_2O_5. The SbO_4 units are formed with mean Sb−O bonds of 0.210 nm. Sb_2O_3 reveals as a good network-forming oxide, better than Sb_2O_5.

1. Introduction

A Sb_2O_3 glass should be formed of the three-fold corner-connected SbO_3 units according to the related crystal structures where the Sb^{3+} cations occupy the apices of trigonal SbO_3 pyramids [1,2]. Zachariasen suspected problems with the ability of pure Sb_2O_3 to form a glass [3]. Distorted SbO_6 octahedra were reported for cubic (c-)Sb_2O_3 [4] at those days. Relevant for comparisons with the glass structure is the polymerized orthorhombic (o-)Sb_2O_3 [1] phase. If in addition to the three bonds of 0.20 nm the Sb−O distances of 0.25 to 0.26 nm are taken into account then each oxygen has three or four Sb neighbors [1]. In fact, pure Sb_2O_3 does not form a glass. Additions of definite glass-formers fix the problem. Glasses from mixtures of Sb_2O_3 and P_2O_5 are possible [5]. The $SbPO_4$ crystal [6] exemplifies such structure. It is formed of SbO_4 and PO_4 units where most oxygens connect exactly two cationic neighbors. The valences of the P−O bonds are 1.25 vu (valence units) on average. Since P=O double bonds do not exist that forces the Sb to form SbO_4 with underbonded Sb−O. The SbO_4 unit is a trigonal bipyramid where the sterically active lone pair of the Sb occupies an equatorial corner. Strictly speaking, the Sb^{3+} is not in the center of the bipyramid but it is shifted a little to that very corner together with its outwards directed lone pair. Glass formation is difficult at the $SbPO_4$ composition itself. The SbO_4 and PO_4 units are not linked randomly. The PO_4 tetrahedron avoids P−O−P linkages as much as possible. Hence, the Sb^{3+} and P^{5+} ions occupy the cationic sites alternatingly and the network structure can crystallize easily due to this preordering. Strong tendency to crystallize exists also for the $AlPO_4$ and $GaPO_4$ compounds of the same stoichiometry.

Glasses $(Sb_2O_3)_x(P_2O_5)_{1-x}$ ($0.95 \geq x \geq 0.65$) were prepared and investigated concerning their thermal, optical and structural properties [5,7-9]. The maximum difference of the glass transition temperature, T_g, and the onset of crystallization, T_x, is obtained with 80 mol% Sb_2O_3 [5,7,8] which indicates the maximum of thermal stability. The glasses show a large transmission window (380 – 2000 nm), large refractive indices of ~2.0 @ 630 nm and small Abbe numbers of ~20 [7]. The nonlinear refractive indices were found up to 50 times larger than that of fused silica [7]. ^{31}P MAS (magic angle spinning)−NMR spectra are interpreted with isolated orthophosphate units (Q^0) [8] that are connected via four corners with Sb as it exists in the $SbPO_4$ crystal. Therefore, they are

also called $Q^{(4)}$ units [8]. Infrared absorption spectra show a transition from Sb_2O_3-like spectra to $SbPO_4$-like spectra with increasing the P_2O_5 content [9]. Raman spectra indicate two types of Sb−O environments, which gradually transform with the compositional changes [8]. The spectra of the ^{121}Sb Mössbauer experiments could be interpreted with the transition from SbO_3 to SbO_4 units toward $SbPO_4$ composition [8]. EXAFS (extended X-ray absorption fine structure) recorded at the K- and L_3-Sb edges was calibrated with spectra of the cubic Sb_2O_3 and $SbPO_4$ crystals [8]. Two Sb−O distances of 0.202 and 0.212 nm with ~2.1 and ~0.7 neighbors revealed to give the best fits. The parameters do not change with the P_2O_5 content which contradicts the other observations. The authors consider it possible that this inconsistency is due to correlations between the Debye-Waller factors and the coordination numbers in the analysis of the EXAFS amplitudes [8].

With the result from ^{31}P MAS NMR of only $Q^{(4)}$ units for the PO_4 in the $(Sb_2O_3)_x(P_2O_5)_{1-x}$ glasses with $x \geq 0.65$ [8] and assuming all O atoms in Sb−O−Sb or Sb−O−P bridges the SbO_3 units must transform to SbO_4 with decreasing x continuously. The Sb−O coordination number, N_{SbO}, should change with

$$N_{SbO} = (2x + 1)/x \quad . \qquad (1)$$

Diffraction experiments are well suited for studying this change. The combination of neutron and X-ray diffraction is useful because an overlap of the lengths of some Sb−O bonds and the O−O edges of the PO_4 could exist. A value N_{SbO} less than predicted could occur if unexpectedly Sb=O double bonds are formed or if some Sb−O bonds a little longer than 0.22 nm are not registered. On the other hand, larger N_{SbO} indicate the existence of three-coordinated oxygen. Such O sites exist in the binary antimony phosphate crystal Sb_5PO_{10} [10] with $N_{SbO} = 3.6$ for $x = 0.83$.

Another point is worth investigating though it is not in the focus of the literature. Sb phosphate glasses rich in P_2O_5 ($x < 0.5$) can be prepared [9,11]. Their infrared absorption spectra indicate the known vibration modes of polymerized PO_4 units [9]. The PO_4 with n tetrahedral corners in P−O−P bridges are called Q^n ($n \leq 3$). Neutron diffraction could resolve two lengths of P−O bonds. Their fractions change with the frequencies of Q^n [12]. The present experiments are aimed at investigating the oxygen environments of the Sb^{3+} ions of the corresponding glasses. It is still an open question whether the value N_{SbO} exceeds the number four. This value could follow the

model expressed by Eq. 1 to reach six for $x = 0.25$ with regular octahedra such as found for N_{GaO} and N_{AlO} in the Ga and Al metaphosphate glasses [13,14]. The binary phosphate glasses with the lone-pair cations Sn^{2+} and Te^{4+} show also the expected changes of the SnO_x and TeO_x units but all their oxygen polyhedra exhibit distortions according to the lone-pair effects [15,16].

2. Experimental

2.1. Sample preparations

The raw materials of glass preparation were phosphorus pentoxide P_4O_{10} (p.a., Merck) and antimony-III-oxide (white, purum, Feinchemikalien Apolda). About 40 g of appropriate mixtures were loaded into SiO_2 glass tubes with diameters of 28 mm which were evacuated and sealed immediately after loading. The ampoules were set in the oven inside a protective container that is filled with sand. After preheating the ampoules were held for melting at 1000 °C for 1 h. Cooling to room temperature took place outside the oven with the ampoules remaining in the protective containers. Melting and storage of the sample materials in ampoules was aimed at minimizing selective evaporation and moisture attack. The ampoules were only broken just before preparing the samples for the measurements. The glassy materials used in the diffraction experiments were taken from the center of the ampoules to minimize any contamination with silica.

An investigation of the full transition from P_2O_5 to Sb_2O_3 glassy networks was planned. Five samples were prepared with Sb_2O_3 contents $x = 0.05$, 0.25, 0.55, 0.80 and 0.95. The samples close to the Sb_2O_3 and $SbPO_4$ compositions revealed to be largely crystallized. The sample of 25 mol% Sb_2O_3 was actually obtained as a clear glass. Unfortunately, the wall of the ampoule broke during cooling and the sample was damaged by humidity. Nevertheless, the results of two good samples are worth presenting. They are named sbp05 and sbp80 according to their x.

2.2. X-ray diffraction

The X-ray diffraction experiments were performed with high-energy photons (HEXRD) at the BW5 beamline of the former synchrotron DORIS III of DESY Photon Science (Hamburg). The incident photon energy was 121.94 keV (wavelength $\lambda = 0.01017$ nm) which was determined by a LaB_6 sample. The glassy powder of the sbp80 and sbp05 samples was loaded into thin-walled

silica capillaries with diameters of 1.5 and 2.5 mm. The beam size was 1x4 mm^2. The scattering intensities were obtained in step-scan mode with a solid-state Ge-detector that was moved horizontally on a straight line. Fluorescence radiation of Sb was removed by an electronic energy window for the detector signal. Intensities were measured in four intervals of scattering angle 2θ (0.5°-5.5°, 5°-10.5°, 10°-15.5°, 15°-27°). Absorbers were used at the small scattering angles to reduce the intensity and, thus, the effects of the detector dead-time. The width of the detector slit was increased at large scattering angles to raise the intensity. Corrections were made for detector dead-time, background, container scattering, polarization, absorption, and the varying sample-detector distance. The scattering intensities were normalized with regard to the atomic structure-independent scattering functions, which were calculated with a polynomial approach [17] of the tabulated atomic elastic scattering factors [18] and atomic Compton scattering data [19]. Finally, the Compton scattering fractions were subtracted and the Faber-Ziman structure factors $S_X(Q)$ [20,21] were obtained as functions of Q that is the magnitude of the momentum transfer with $Q = (4\pi/\lambda)\sin\theta$.

2.3. Neutron diffraction

The neutron diffraction experiments (ND) were performed at the GEM instrument of the spallation source ISIS of the Rutherford Appleton Laboratory (Chilton/ UK). The powdered sample material was loaded into thin-walled vanadium cylinders (diameter, 8.3 mm). The duration of the data acquisition was at least three hours per sample. A vanadium rod (diameter, 8.4 mm) was used to determine the incident energy spectrum which is needed for the data normalization in the time-of-flight regime. The data were corrected using standard procedures for the container and background scattering, attenuation, multiple scattering and inelasticity effects [22]. The differential scattering cross-sections of the detector groups 2, 3, 4, and 5 with scattering angles of 14°-109° were normalized to the calculated mean scattering that was calculated from the tabulated neutron scattering lengths. Finally, the neutron Faber-Ziman structure factors, $S_N(Q)$ were obtained [20,21].

3. Results

3.1. Structure factors and real-space correlations

The final X-ray and neutron structure factors, $S_N(Q)$ and $S_X(Q)$, are shown in Fig. 1 by means of the weighted interference functions $Q\cdot[S(Q)-1]$. Both the structure factors of sbp05 are similar with those reported for vitreous (v-)P_2O_5 where the first sharp diffraction peaks (FSDP) appear also as double maxima [23]. Obviously, the addition of 5 mol% Sb_2O_3 does not change the main features of the medium-range order of v-P_2O_5. The neutron structure factor $S_N(Q)$ of the sample sbp80 shows a double maximum of FSDP, as well, which may indicate a similar medium-range order. On the other hand, the $S_X(Q)$ of sbp80 has a single first peak at ~20 nm^{-1}. If one looks carefully on its left flank one finds a small shoulder at ~13 nm^{-1} (cf. also Fig. 4, Chapter 4.1). Presumably, the strong X-ray scattering power of the Sb atoms modifies the contrast clearly which is accompanied with strong changes of the total scattering intensities.

The real-space correlation functions $T_N(r)$ and $T_X(r)$ were obtained by Fourier integral over the corresponding $S_k(Q)$ factors with

$$T_k(r) = 4\pi\, r\rho_0 + \frac{2}{\pi}\int_0^{Q_{max}} Q[S_k(Q)-1]\, M(Q)\sin(Qr)\, dQ \quad . \qquad (2)$$

The number densities of atoms, ρ_0, were calculated from the glass compositions and the mass densities [10] with 70 nm^{-3} from 2.5 g/cm^3 for sbp05 and 59 nm^{-3} from 4.8 g/cm^3 for sbp80. The Q_{max} were chosen with 450 nm^{-1} (ND) and 273 nm^{-1} (HEXRD). A damping factor $M(Q)$ according to Lorch with

$$M(Q) = (Q_{max}/\pi Q)\sin(\pi Q/Q_{max}) \qquad (3)$$

was used. Damping reduces the spurious ripples of the correlation functions that are due to the noise in $S(Q)$ at large Q-values (cf. Fig. 1) and the termination of the Fourier integral at Q_{max}. Damping broadens the peaks, which could smear out some distance details. The functions $T_k(r)$ are shown in Fig. 2. The partial contributions of the different atom pairs depend on the weighting factors (Table 1) where scattering power and mole fractions of the corresponding atomic species determine these weights. The weighting factors of HEXRD are given as constants for qualitative comparisons. Actually, the analysis was performed with the Q-dependent X-ray factors.

The $T_k(r)$ curves of sample sbp05 show clear P−O and O−O peaks, which belong to the bonds and edges of the PO_4 tetrahedra. The Sb−O peak is not visible in the $T_N(r)$ curve due to the small

Sb_2O_3 content while the strong X-ray scattering of Sb is sufficient to produce a significant Sb−O peak in $T_X(r)$. The peak at ~0.34 nm in the $T_X(r)$ is presumably due to Sb−P distances. A similar peak does not occur for v-P_2O_5 [23].

The $T_k(r)$ curves of sample sbp80 show clear Sb−O peaks due to their large weights (Table 1). The $T_N(r)$ shows a separate P−O peak. The distances of the tetrahedral O−O edges at 0.252 nm overlap with numerous longer distances in the range from 0.26 to 0.29 nm which must belong to the O−O or Sb−O correlations according to their strong weights. The special geometries of the SbO_3 and SbO_4 units have small O−Sb−O angles that correspond to short O−O edges. Such as in the related crystals a SbO_3 has three short O−O edges [1,2] while a SbO_4 has five short edges [6]. The $T_X(r)$ curve of sbp80 shows small P−O and O−O peaks that do not allow extracting the coordination numbers. The strong Sb−O peak at 0.20 nm is followed by a constant plateau up to distances of 0.31 nm. Due to small weight of the O−O partial correlations in the $T_X(r)$ the O−O edges of the PO_4 and SbO_x units can provide only part of this distribution. A source of other distances is the Sb−O correlation. Some Sb−O distances comparable with those at ~0.26 nm of o-Sb_2O_3 [1] and a little longer should exist. Finally, the large weight of the Sb−Sb correlations heightens the peak at ~0.35 nm. It belongs to the corner-connected SbO_x units of the antimonite network.

3.2. Short-range order parameters

Gaussian fitting of the first-neighbor peaks was performed simultaneously to the $T_N(r)$ and $T_X(r)$ data to determine the atomic distances and coordination numbers. The effects of truncation at Q_{max}, damping and the Q-dependent partial weighting factors were taken into account [24-26]. The parameters of the peaks up to O−O at 0.252 nm were determined by least-squares fitting procedures. Peaks of larger distances were modelled with reasonable parameters or adjusted by hand. The foothills visible in the $T_X(r)$ on both sides of the O−O peak (Fig. 2a) and the Sb−O peak (Fig. 2b) are not real distances but they appear due to the Q-dependencies of the X-ray weighting factors. Table 2 lists the resulting parameters from the fits while Table 3 resumes the total coordination numbers and the mean distances.

Two Gaussians approximate the P−O peak of sample sbp05. The difference of both distances

was fixed. The P=O double bonds of the Q^3 and the two non-bridging bonds of the Q^2 contribute to the short P−O bonds while the single bonds of the P−O−P bridges contribute to the longer P−O bonds [12]. The length of the tetrahedral O−O edges was fixed with 0.252 nm as known of v-P_2O_5 [23]. Though the Sb−O peak is small a reliable coordination number of 4.1±0.4 with a mean distance of 0.210 nm is determined. Thus, SbO_4 pyramids rather than SbO_6 octahedra or SbO_3 pyramids exist. The P−P and Sb−P peaks are found at 0.295 nm and 0.34 nm such as expected for SbO_x units in phosphate networks.

Sample sbp80 contains still sufficient PO_4 to determine clear P−O and O−O distances in the $T_N(r)$ curve. Though only isolated PO_4 with four P−O−Sb bridges exist [8] two different distances are used to approximate the P−O peak. For reasons of charge balance, the PO_4 units are linked to the SbO_4 units. The SbO_4 are trigonal bipyramids as found in the $SbPO_4$ or Sb_5PO_{10} crystals [6,10]. Hence, it is impossible to find four equally strong bond partners for a PO_4. Strong P−O bonds balance the two weak axial Sb−O bonds of the SbO_4 bipyramid while weaker P−O bonds link to the equatorial O corners of the SbO_4 or any O corners of the SbO_3 units.

The length of the O−O edges of the PO_4 was fixed such as for sample sbp05. The number of O−O neighbors found at this distance is 1.46, which is the average for all O atoms. To calculate this N_{OO} value for a given glass composition it is not needed knowing the oxygen fractions of different functionality. It is sufficient considering the numbers of PO_4 units with their six edges. Each edge has to be counted twice because it is seen from the oxygens of both ends. Thus, N_{OO} is the ratio of two times the number of all PO_4 edges to the total number of the oxygens which is

$$N_{OO} = 24(1 - x)/(5 - 2x) \quad (4)$$

for the Sb phosphate glasses. The calculated N_{OO} for sbp80 is 1.41 which is close to the value from the fit (Table 2). The calculated N_{OO} of sbp05 is 4.65 which is also close to the fit result.

The Sb−O peak is approximated with three Gaussians. The longer Sb−O bonds of 0.228 nm with 0.5 neighbors belong to the SbO_4 units. The same number of short Sb−O bonds completes the SbO_4 and the portion 1.0 of N_{SbO} means 25% Sb in SbO_4 units and, hence, a total N_{SbO} of 3.25. That agrees with the calculated value from Eq. 1. The total N_{SbO} from the peak area is 3.3±0.2 (Table 3). These results are consistent with the model of corner-connected SbO_3, SbO_4

and PO_4 with all oxygens in either Sb−O−Sb or Sb−O−P bridges.

The broad peak at 0.28 nm in the $T_N(r)$ that occurs beyond the O−O distances of the PO_4 edges (cf. Fig. 2b) is related to the short O−O edges of the SbO_3 and SbO_4 units. Planar SbO_3 triangles with Sb−O bonds of 0.200 nm would show edge lengths of 0.346 nm. Regular SbO_4 tetrahedra with the same bond lengths would form edges of 0.325 nm. The short O−O edges of 0.280 nm correspond to O−Sb−O angles of ~90°. Such angles are known of the SbO_3 and SbO_4 pyramids in the crystals o-Sb_2O_3 [1] and $SbPO_4$ [6] with values close to 90° and 85°, respectively. The Sb^{3+} cation of the SbO_3 pyramid lies 0.118 nm distant to the base (cf. Fig. 3) with angles of 36.1° between the Sb−O bonds and the base. An O−Sb−O angle of 90° reminds a well-known structural unit, namely the regular octahedron. The natural example for comparison is the SbO_6 octahedron of the Sb_2O_5 crystal [27] with an average length of the Sb−O bonds of 0.199 nm. The SbO_3 and SbO_4 of our glass can be derived from that SbO_6 by replacing three oxygens (one face) or two oxygens (one edge), respectively, with the lone pair. For the SbO_4, subsequently, the two each other most distant oxygens are shifted a little outwards with a small tilt away from the lone pair.

The calculation of the N_{OO} of the O−O distances at ~0.28 nm is running similar to Eq. 4. In the case that only SbO_3 pyramids (three O−O edges) exist their N_{OO} number is obtained with

$$N_{OO} = 12x/(5 - 2x) \quad . \tag{5}$$

Five short edges must be taken into account for a trigonal SbO_4 bipyramid. The fraction of SbO_4 increases with decreasing x according to Eq. 1 and one obtains $N_{OO} = 4$ for $x = 1$, $N_{OO} = 3.3$ for sbp80 with 25% Sb in SbO_4 and $N_{OO} = 2.5$ for the $SbPO_4$ composition. Trigonal SbO_4 bipyramids for sample sbp05 correspond to an N_{OO} contribution of 0.2 at 0.28 nm. Possibly, these distances contribute to the difference of the calculated number of the PO_4 edges. The value N_{OO} of the PO_4 was found by 0.2 too large (cf. Table 2).

Considering the scattering weights of the pair correlations of sample sbp80 (Table 1) the O−O distances are strongly represented in the $T_N(r)$ but they contribute only little to the $T_X(r)$. Here, the O−O contribution is too small for the distance range 0.26 nm ≤ r ≤ 0.30 nm. Other distances in this range that have sufficient weight belong to the Sb−O partial correlation. The combination

of the $T_N(r)$ and $T_X(r)$ data allows separating the O−O and Sb−O correlations. The first Sb−P and Sb−Sb peaks at 0.33 nm and 0.35 nm are taken into account because their flanks influence the distance distributions at ~0.29 nm in the $T_X(r)$. These peaks belong to corner-connected network groups. The numbers of neighboring groups for sbp80 are chosen for the case of 25% Sb in SbO_4. One finds N_{SbP} = 1.0 and N_{SbSb} = 2.25 according to the model assumptions of Eq. 1.

Finally, the O−O and Sb−O correlations are extracted up to 0.30 nm. The Sb−O correlation is small for 0.24 nm ≤ r ≤ 0.28 nm, but not negligible. Significant numbers of Sb−O distances occur at 0.29 nm. Sb−O distances larger than 0.30 nm are not accessible to this approach. The number of the O−O distances found at 0.28 nm is 3.9. That is larger than the 3.3 expected for the short O−O edges of the SbO_x units. Missing second-neighbor P−O distances of $r \geq 0.30$ nm could lead to a larger value N_{OO}. Moreover, O−O distances of $r \geq 0.30$ nm may already exceed the edge lengths and can belong to different SbO_x units.

The Sb−Sb distance of the large peak seen in the $T_X(r)$ function is ~0.35 nm. Supposing, the oxygen triangles of the connected pyramids are forming flat layers and the Sb are by 0.12 nm outside the layers. If the Sb sites of neighboring triangles would point to the same side of a layer that would lead to short Sb−Sb distances of ≤0.32 nm. Their mutual repulsion would tilt away the triangular bases. An example of this behavior is the Sb_4O_6 molecule of the c-Sb_2O_3 [2] with Sb−Sb distances of 0.362 nm. Such structures could not accept other units such as SbO_4 to form a continuous glassy network. Alternatively, the apices of the corner-linked SbO_3 pyramids could point alternately to both sides (cf. Fig. 3). Such changes of orientation require rings of even numbers of units as found in the o-Sb_2O_3 crystal [1] with four-membered rings. Bridges Sb−O−Sb connect the Sb sites of adjacent SbO_3. With Sb−Sb distances of 0.35 nm and Sb−O bonds of 0.20 nm the bridging angle is 122°. Straight chains of SbO_3 units would lead to larger angles. The o-Sb_2O_3 crystal [1] has two different angles close to our result, namely 116° and 131°. They belong to the four-membered rings of the SbO_3 that connect to double chains.

3.3. Bond valences of the Sb−O bonds

Structural considerations based on the ionic radii are inappropriate for the Sb^{3+} cation with its sterically active lone pair. SbO_x groups of related crystal structures are helpful for interpretations.

The concept of bond valences is a possible approach to assessing the reliability of the measured short-range order parameters [28]. The bond valence sums (*BVS*) of all Sb−O bonds of a given Sb site should equal the nominal valence of the Sb^{3+} cation which is also expected for the average of all Sb sites of a glass sample (parameters in Table 2). Brown & Altermatt [28] related the bond valence bv_{ij} (bond strength) of a given bond to its length r_{ij} by

$$bv_{ij} = \exp\left[\left(\mathrm{R}_0 - r_{ij}\right)/\mathrm{b}\right] \quad . \tag{6}$$

Eq. 6 is robust and widely applicable that the parameters R_0 and b were improved for many atom pairs up to these days. R_0 is a measure of the size of the two ions and b expresses the softness of their interaction. Earlier, a fixed value b = 0.37 Å was used [28]. Large varieties of lengths exist for the Sb−O bonds due to the lone-pair effects. Eq. 6 must be valid for lengths from 0.18 to 0.35 nm. Mills et al. [29] and Gagné & Hawthorne [30] determined the parameters with great care. Here, the values R_0 = 1.932 Å and b = 0.435 Å [30] are used for calculating the valences of the Sb(III)−O bonds. The parameters of [29] are nearly identical.

At first, the sums of bond valences (vu) of the Sb−O distances of the related crystal structures are calculated. The values *BVS* are 3.01 vu for o-Sb_2O_3 [1], 3.00 vu for c-Sb_2O_3 [2], 3.13 vu for $SbPO_4$ [6] and 2.98 vu (average) for Sb_5PO_{10} [10] where all Sb−O distances up to 0.35 nm are taken into account. The *BVS* of most Sb^{3+} containing structures were found within (3.0±0.1) vu [29]. This interval characterizes the uncertainty of the approach.

The *BVS* of 2.84 vu determined for the glass sbp05 is close to the nominal value. The *BVS* of the glass sbp80 with taking into account only Sb−O distances < 0.24 nm is smaller with 2.62 vu. The full environments of the Sb^{3+} in SbO_3 or SbO_4 pyramids are not formed of only three or four oxygens. As examples, the complete oxygen environments of the five independent Sb sites of the crystal structure Sb_5PO_{10} were given in [10]. Numerous Sb−O bonds have lengths of ~0.20 nm while, beyond a gap around ~0.25 nm, further distances pile up at ~0.30 nm. The solid angle around the Sb^{3+} cation is divided into that half on side of the sterically active lone pair and the other half in opposite direction. All bonds to the opposite side of the lone pair are called primary bonds with r_{SbO} < 0.24 nm. The long distances on side of the lone pair are the secondary bonds (or non-bonding distances) which, in the limit, contribute only marginally to the *BVS* (0.025 vu at

0.35 nm). The calculation of the *BVS* of the Sb_5PO_{10} crystal for the primary bonds results to 2.69 vu which is close to the 2.62 vu obtained for the glass sbp80. The remaining 0.38 vu must belong to secondary Sb−O bonds. The experimental determination of the longer distances is difficult for the glasses. The analysis of the $T_N(r)$ and $T_X(r)$ curves of sbp80 (Fig. 2b) provided only part of the secondary bonds for 0.25 nm < r < 0.30 nm with 1.4 neighbors. Their contribution to the *BVS* is 0.17 vu. Possibly, the number of Sb-O distances at ~0.29 nm is already too small. We do not have access to the Sb−O distances between 0.29 nm and 0.35 nm.

The largest lengths of 0.228 nm of the primary Sb−O bonds of sbp80 have bond valences of 0.5 vu. Axial bonds of a SbO_4 trigonal bipyramid possess such lengths, which indicate the small fraction of SbO_4 units. One would expect similar bond lengths for a regular SbO_6 octahedron. The bond lengths of the SbO_x units of sample sbp05 are smaller which confirms the interpretation with SbO_4 units. The two different characteristic bonds in equatorial and axial directions of the trigonal bipyramids SbO_4 are, however, not resolved for sample sbp05.

It was stated in the previous section that the SbO_3 pyramid reminds a half SbO_6 octahedron with bond lengths of 0.199 nm. One obtains a *BVS* of 2.62 vu for the primary bonds as already calculated from our experimental data of glass sbp80. For the SbO_4, a similar *BVS* is obtained after a small increase of the bond lengths. Obviously, the Sb^{3+} cation behaves such as a Sb^{5+} cation on the side of its primary bonds while bonds are widely suppressed to the other side (only small contribution of bond valence).

4. Discussion

4.1. Low-Q features of the scattering intensities

The neutron diffraction curves of both samples (cf. Fig. 1) show similar double peaks in the range of the FSDP (Q < 25 nm^{-1}) that are related to characteristics of their medium-range order. Fig. 4 shows these features of the low-Q ranges of the neutron and X-ray structure factors quite clearly. The medium-range order of sample sbp05 (only one antimonite unit per 19 PO_4 units) should be similar to that of v-P_2O_5. Such double maxima are well known of v-P_2O_5 [23]. On the other hand, differences to the network structure of o-Sb_2O_3 [1] are expected for sample sbp80 with ratios of 1:1:3 of the PO_4, SbO_4 and SbO_3 units. Hence, it is surprising that the first scattering

peaks of this glass are found at the positions of the first major Bragg-reflections of o-Sb_2O_3 [1]. Their *Q*-values are shown with vertical lines in Fig. 4. The c-Sb_2O_3 [2] does not possess similar reflections. However, one would not expect lattice planes in the glass that meet exactly the order of the related crystal. This point needs closer inspection.

At first, it is focussed on sbp05 and P_2O_5. It is remembered the interpretation of the medium-range order of v-P_2O_5 where it was compared with the two orthorhombic forms of P_2O_5 [31,32]. Infrared and Raman spectroscopy on v-P_2O_5 show greater similarity with the spectra of o'-P_2O_5 than those of o-P_2O_5 [33,34]. The reverse Monte Carlo (RMC) simulations of v-P_2O_5 yielded a bridging angle P−O−P close to 141° [23] which equals that of o'-P_2O_5 [32]. The partial structure factor $S_{PP}(Q)$, however, as calculated from the RMC structures [23], has its first maximum at 13 nm^{-1} which agrees with that calculated for o-P_2O_5 [31]. Here, Fig. 5a shows a comparison of the double maxima of the FSDP of sample sbp05 with the broadenend Bragg-reflections of o-P_2O_5 and o'-P_2O_5. The two maxima of the glass sbp05 agree with the positions of the prominent (111)- and (240)-reflections of o-P_2O_5 which are indicated with vertical lines. The first strong reflection of o'-P_2O_5 appears at larger *Q* than the first maximum of the glass. One can try identifying the structures in the crystal lattices that are responsible for the Bragg peaks. A view along the (111)-layers of o-P_2O_5 reveals longish cavities. Few PO_4 units link the upper and lower layers of these network cavities. The cavities are filled with the P atoms and their doubly bonded oxygens. Packaging issues play a key role for the medium-range order of v-P_2O_5 (and sbp05). The (111)-reflection of o-P_2O_5 is the corresponding interference. Structural features perpendicular to the direction of the stacking of the layers cause the second maximum at ~21 nm^{-1}. Identifying the structural components that are responsible for this second maximum is difficult.

A comparison of the low-*Q* maxima of the sbp80 glass with the powder pattern of broadened reflections of o-Sb_2O_3 [1] and Sb_5PO_{10} [10] crystals is shown in Fig. 5b. The change of contrast of the neutron and X-ray diffraction curves is well visible in changed peak heights for the crystals and the glass likewise. Better agreement for the glass exists with the powder pattern of o-Sb_2O_3. The vertical lines indicate three Bragg-reflections of this crystal. The (040)-reflection is close to the (121)-peak. It is not shown separately. The (040)-reflection corresponds to the periodicity of

the Sb sites in the double chains of the SbO_3 units. These periods cause the strong interference at 20 nm^{-1} in $S_X(Q)$. The double chains of o-Sb_2O_3 are formed of four-membered rings of SbO_3 pyramids such as that shown in Fig. 3. Again, we cannot clarify the origin of the second maximum (at 20 nm^{-1}) of the glass unequivocally.

On the other side, the double chains are oriented along the (110)-layers and one can relate the distance of $2\pi/Q_1$ = 0.457 nm between these lattice layers to the diffraction peak at Q_1 = ~13 nm^{-1} in the $S_N(Q)$ data. Why does this peak just appear as a tiny shoulder in the $S_X(Q)$ data? The network layers are mainly formed of the oxygen atoms of the pyramidal bases of the SbO_3 units. The Sb sites are situated outside the layers and alternately to both sides. Accordingly, the Sb−Sb correlations do not reproduce the stacking of the layers. The Sb atoms are strong X-ray scatterer but do not contribute significantly to the first peak at 13.8 nm^{-1}.

The composition of the sbp80 glass is close to that of the Sb_5PO_{10} crystal [10] (x = 0.83) but its fraction of Sb in SbO_4 (60%) is clearly larger than in the glass. The layers of the crystal are formed of either three-membered rings or PO_4-SbO_4 pairs which is only little reminiscent of the o-Sb_2O_3 structure. The authors of Sb_5PO_{10} [10] emphazise that other binary antimonite crystals show that stacking of layers of SbO_3 units which exists in the o-Sb_2O_3 crystal. That finding supports our interpretation for the sbp80 glass that layers similar to those of o-Sb_2O_3 are still possible.

One can resume, that the medium-range order of the glasses sbp05 and sbp80 is given by a stacking of network layers that are formed of connected oxygen triangles. These triangles are the bases of PO_4 tetrahedra (Q^3 groups) for sbp05 or the bases of SbO_3 pyramids for sbp80. The distance between the layers for sample sbp05 is $2\pi/Q_1$ = ~0.46 nm according to the position Q_1 of the first diffraction peak at 13.5 nm^{-1}. The terminal O sites of a PO_4 are distant to the bonded base of the tetrahedron by ~0.22 nm. The remaining distance (0.24 nm) to the other side is determined by oxygens that do not belong to the same PO_4 and that should be ≥0.30 nm. Therefore, the bases of the PO_4 units must be tilted to the layer plane that there is enough space for these oxygen sites. The distance between the layers for sample sbp80 is ~0.48 nm according to the position of the first diffraction peak at 13.0 nm^{-1}. The interstices are filled with the Sb^{3+}

cations and the largest part is mainly due to the effects of their lone pairs. The Sb sites are ~0.12 nm outside the pyramidal base of the SbO_3. The remaining 0.36 nm are spanned by the long non-bonding Sb−O distances on side of the sterically active lone pairs.

4.2. The evolution of the structural units and their linkages

Binary antimony phosphate glasses can be prepared in a large range of composition. Glasses close to the pure Sb_2O_3 and $SbPO_4$ compositions are not possible. Zachariasen's rules of glass formation [3] would not contradict the formation of these glasses. However, additional constraints of special network linkages are effective. The strong attraction of the four PO_4 corners to SbO_4 corners in case of equal numbers of P and Sb ($SbPO_4$) causes the network flexibility to fall below the needed level for glassy disorder. For the networks of pure Sb_2O_3, the mutual repulsion of the Sb^{3+} lone pairs of the corner-connected SbO_3 favors the formation of four-membered rings (Fig. 3). The layered structures that remind those of o-Sb_2O_3 exist already in sbp80. Obviously, the crystallization to o-Sb_2O_3 is not to avoid without sufficient disturbing groups and linkages (lattice defects).

The magnitudes of the parameter of the ^{31}P NMR spin echo decay of the $SbPO_4$ crystal [6] and the $(Sb_2O_3)_x(P_2O_5)_{1-x}$ glasses of $0.90 \geq x \geq 0.65$ indicated that certain P−P correlations exist [8]. P−O−P bridges were excluded by ^{31}P MAS NMR [8]. The decay parameters obtained for the glasses were similar to that of the crystal and they did not change with x. The corresponding P−P correlations must exist throughout all glass compositions. The two weak axial Sb−O bonds of a SbO_4 unit connect two PO_4 units. Also, each PO_4 needs two axial Sb−O bonds for charge balance. Both constraints cause PO_4−SbO_4 chain structures to be formed as shown in Fig. 6. Other PO_4 may be connected to the equatorial corners of the SbO_4. This is the situation in the $SbPO_4$ and Sb_5PO_{10} crystals [6,10] and also expected for the glasses. The shortest P−P distance of the $SbPO_4$ crystal [6] is 0.41 nm. It is only a little longer (0.42 nm) in the Sb_5PO_{10} crystal [10]. SbO_4 units could be stabilized also with two axial corners forming a three-coordinated oxygen with an O corner of a SbO_3 unit. Such O sites exist in the Sb_5PO_{10} crystal [10]. In this case, N_{SbO} would be larger than given by Eq. 1. Such oxygens do exist in the glasses only as minor fractions in the limits of the uncertainty of N_{SbO} and would not change the P−P correlations.

The PO_4 networks of phosphate glasses are commonly disrupted using all available oxygen [35] which is proven also for the Sb_2O_3-P_2O_5 system [8,9]. In this process, the PO_4 units avoid the P=O double bond as much as possible, even that of a Q^3 group, by all non-bridging oxygens (NBO) coordinating a cation of the second species M^{z+} [36]. This leads to bridges P−O−M and characteristic changes of the N_{MO} values vs. modifier content x. The Sb_2O_3-rich glasses prefer forming networks of SbO_3 units with Sb−O−P and Sb−O−Sb bridges. Three-coordinated oxygen can exist throughout all glass compositions only in marginal fractions.

The results of the glass sbp80 follow this behavior. On the other hand, the Sb_5PO_{10} crystal [10] of similar composition has a considerable amount of three-coordinated oxygen. Also the SbO_3 units in the o-Sb_2O_3 crystal [1] have two secondary bonds of ~0.26 nm while only 0.3 Sb−O bonds of similar length were found for the glass sbp80. However, the first diffraction peaks of sample sbp80 indicate a medium-range order similar to that of o-Sb_2O_3 (stacked layers).

The structure of the glass sbp05 is formed of SbO_4, Q^2 and Q^3 units in a numerical ratio 1:3:16 according to the known degradation of phosphate networks due to modifier additions [35]. The sbp05 represents an example of the first part of *Range I* of the model of phosphate glasses [36]. This range is characterized by an excess of terminal oxygens. Not all NBO's can get close to a Sb^{3+} cation. The mean Sb−Sb distance is too long that both NBO of a Q^2 group could approach two Sb^{3+} sites. It is not expected, that the NBO edge of the Q^2 points to a Sb^{3+} site. Three NBO's of three Q^2 and a P=O corner of a Q^3 could form the primary bonds of a SbO_4 unit of glass sbp05. This behavior does not allow to conclude for the SbO_x units in the upper part of *Range I* and the first part of *Range II* ($0.15 \le x \le 0.40$). Due to smaller Sb−Sb distances, the two and three NBO's of the Q^2 and Q^1 can link different Sb^{3+} sites. Four-, five- or six-coordinated Sb could be formed according to Eq. 1 with all NBO's in Sb−O−P bridges. On the other hand, all the SbO_x units are expected with sterically active lone pairs that limit the number of primary bonds to four. The inspection of numerous antimonite crystals reported in [29] finds most Sb^{3+} cations with three Sb−O bonds of 0.20 nm and secondary bonds of 0.31 nm. Other Sb^{3+} have four Sb−O bonds of 0.19 nm < r_{SbO} < 0.24 nm. Few SbO_x units of indifferent distortions exist but never units of five or more primary bonds (< 0.24 nm).

The P−NBO of the Q^2 and Q^1 units have, on average, bond valences of 1.5 vu and 1.33 vu, respectively. Hence, in case of SbO_4 units it is needed to move bond valence from some P−NBO to primary Sb−O bonds and, in return, from secondary Sb−O to other P−NBO. That results in unequal P−NBO of a given Q^2 or Q^1 unit. The SbO_4 was assumed as a trigonal bipyramid with two short and two longer bonds (Fig. 6) as in $SbPO_4$ [6]. Some SbO_4 units of Sb_5PO_{10} [10] show other variations of bond lengths. Thus, predictions of the SbO_4 units of glasses with Q^1 and Q^2 are difficult. Few Sb−O distances up to 0.28 nm (secondary bonds) are expected to balance the deficits of bond valences of primary bonds. A portion of the Q^2 and Q^3 groups will have terminal P=O double bonds and, hence, the corresponding glasses are hygroscopic.

When considering the abilities of glass formation of a given oxide, the criteria of field strength according to Dietzel [37] are often used. This concept does not take care of distorted structural units. As pointed out in the Results chapter the structural SbO_3 and SbO_4 units remind to the SbO_6 octahedra of the Sb^{5+} cations in the Sb_2O_5 crystal [27]. By using the length of the Sb-O bonds for the SbO_3 pyramid (a = 1.99 Å [27] and Z = 5) one finds Z/a^2 = 1.26 e/Å^2 which means good network-former property. The value is reduced to 1.10 e/Å^2 for the SbO_4 unit due to the elongated bonds. The Sb_2O_5 itself could be assumed as a good network-former oxide according to that field strength. However, the Sb^{5+} with six oxygen neighbors contradicts Zachariasen's rules of glass formation [3]. It is paradox but the reduced oxidation state optimizes the network-former properties of Sb^{3+} with still strong field strength but small numbers of bonds. That means three or four strong Sb−O bonds per network unit and all oxygens in bridging sites. This point of view is close to the ideas on the lone-pair effects in the bond valence model of Brown [38] (next chapter).

4.3. General remarks on the $5s^2$, $6s^2$ lone pair elements in glassy networks

Several main group elements of high periodic numbers often do not appear with their nominal oxidation state but with a state reduced by two and the pair of non-bonding electrons is assigned to the outer *s*-orbital. The geometries of the oxygen polyhedra coordinating the cations M^{z+} = Sn^{2+}, Sb^{3+}, Te^{4+}, Pb^{2+} can show steric effects from these non-bonding valence electrons. The shapes of polyhedra of different numbers of ligands were derived from stereochemical point of

view [39] where the lone pairs were considered as additional ligands (also the $5s^2$, $6s^2$ electron pairs). The repulsions based on the electrical charges were assumed stronger for the lone pairs than for the oxygen ligands which explains the reduced O−M−O angles.

Orgel [40] attributed the origin of the steric effects of the *s*-electrons of the cation to the mixing with its empty *p*-states. That is possible due to the small energy gap. However, mixing of *s*- and *p*-states requires non-symmetric environments. The estimation of the needed energy was based on a simple polarization model. If the gain in M−O bonding energy supplies the promotion energy from *s*- to *p*-orbitals, then regular environments are unstable [40]. The effect increases with decreasing cation-anion distances. It is large for the O^{2-}, F^- anions.

The classical explanations of the steric lone-pair effects are based on electrostatic repulsions [39]. However, conventional electron-density mapping does not show aspheric distributions that could give rise for such repulsions. Ab-initio methods (density functional theory – DFT) used to map the electron densities of, for example, the SnO_4 or PbO_4 pyramids in SnO and PbO litharge crystals show spherical distributions of the valence electrons of the cations [41]. The electron localization function was used to visualize the non-bonding part of these distributions. Spherical caps were identified on side of the lone-pair [41]. This spin-paired electron density causes strong repulsions. DFT methods were used to study the details of the mechanisms of covalent bonding in the corresponding compounds. Many own and other results are summarized by Walsh et al. [42]. The cation s^2 electrons interact with the anion *p* states which results in low bonding and higher anti-bonding states. Distortions of the cationic environments allow the cation *p* states to hybridize with these anti-bonding states, which stabilizes the occupied states. Other authors [43] argue that the anion *p* orbital has only small effects on the hybridization.

Applications of DFT on the lone-pair effects are time-consuming calculations. DFT was never used for lone-pair effects in glass networks. Alternatively, simple estimations such as the bond valence model [38] are applicable. The bond valence model follows the main DFT results. The lone pairs are stereochemically inactive in their natural state. The total electron density of atoms is spherical irrespective of the stereochemical effects. The reordering of the non-bonding part of electron density to one side of the $5s^2$ or $6s^2$ cation is due to the needs of special anions for

strong bonds that point to the opposite side. The bond valence – bond length relation of distorted polyhedra shows a special behavior [38]. The change of bond valence (increase and decrease by the same amount) of a given M−O bond leads to clearly less shortening if compared with its lengthening (cf. Eq. 6). Hence, the average bond length of a given structural unit increases with its distortion. This may explain the large distance of 0.48 nm between the oxygen layers found for the glass sbp80 though the distance of the Sb^{3+} to the layer of strong bonds is only 0.12 nm. The analysis of the volumes of the oxygen polyhedra of numerous Te^{4+} sites in crystals revealed interesting specifics [44]. (i) The oxygens that surround the Te^{4+} sites are located close to the surfaces of spheres whereby the radii of spheres vary from 0.24 to 0.30 nm. The oxygens are distributed unevenly on these surfaces. (ii) The distances between the centers of spheres and the Te^{4+} sites vary from 0.08 to 0.15 nm. They follow the radii of spheres in a linear relationship. These findings show the possibilities and limits of structural modelling of the corresponding glasses.

Special crystal symmetries can force a M^{z+} cation to accept symmetric oxygen environments. However, disordered networks of glasses always tend to destabilize symmetric environments. The type of distorted oxygen polyhedron can of course vary. The number of primary bonds may change and secondary bonds can contribute bond valence significantly. The available numbers and charges of the oxygen ligands determine the type of SbO_x unit. The tendency of oxygen for bridging sites is another constraint and generally valid for glass networks [3]. The latter stabilizes the SbO_3 units in the glass sbp80 for 75% of the Sb. The PO_4 units demand Sb−O bond valences less than unity. Hence, SbO_3 units are no more stable with increasing phosphate content.

Similar changes of the structural units with sterically active lone pairs are already known of phosphate glasses containing SnO [15] and TeO_2 [16]. Units of even five primary bonds were detected in the case of TeO_2 ($N_{TeO} > 4$) [16] such as known of the $Te_2O(PO_4)_2$ crystal [45]. TeO_3 units with a Te=O double bond are supposed with a minor fraction in vitreous TeO_2 [46]. Analogous SbO_3 are not expected because of the needed large differences of bond valences to the three Sb−O ligands. The predicted bond valence problem of the Sb^{3+} with Q^2 and Q^1 groups (Chapter 4.2) exists also for the Sn^{2+} with the Q^3 and Q^2 groups [47]. The expected fractions of

the Q^3 and Q^2 were found by ^{31}P NMR but due to broad signals their determination needed special 2D techniques [47]. The SnO_4 trigonal bipyramids cause broad distributions of bond valences of the P−NBO bonds of the Q^2 and Q^3. The analysis of the ^{119}Sn NMR signal in this compositional range was difficult [47] because the SnO_4 unit of only one crystal is available for comparisons.

Significant changes of the PbO_x polyhedra were found in glasses of different network formers [48]. The steric effects of the lone pairs of Pb^{2+} cations are strong in silicate glass while they appear reduced in phosphate environments. Even the germanate anomaly influences the PbO_x environments [49]. These effects are attributable to a change of the oxygens from bridging to non-bridging character when the PbO content exceeds 25 mol%. The Empirical Potential Structure Refinement was used to generate atomistic models of a PbO-rich silicate glass [50]. The Pb^{2+} lone pairs were introduced by negative point charges fixed by 0.10 nm distant of the Pb^{2+} sites. The corresponding potential produces, similar to the spheres found for the Te^{4+} environments of crystals [44], oxygen positions on spherical surfaces around the lone pairs, however, without variations of the radii. The special simulation of the lone pair was taken from lone-pair localization calculations of lead containing crystals, where electrostatic interactions were sufficient to reproduce the stability criteria of the crystal structures [51].

5. Conclusions

Antimony phosphate glasses $(Sb_2O_3)_x(P_2O_5)_{1-x}$ can be prepared in a large range where only glasses close to the Sb_2O_3 and $SbPO_4$ compositions are not obtained. Samples with an excess of P_2O_5 need melting in sealed ampoules. Two samples (x = 0.05 and 0.80) were measured by neutron and X-ray diffraction with large Q-ranges that provide good real-space resolution.

The P−O and O−O distance peaks indicating the lengths of the PO_4 tetrahedra are found with the expected numbers of neighbors for the two glasses studied. For the glass sbp80 the Sb−O and O−O coordination numbers and distances of the SbO_3 and SbO_4 pyramids indicate strong distortions of the units that are due to sterically active lone-pairs of the Sb^{3+} cations as known of the related crystals. The fraction of SbO_4 pyramids matches the right portion, that all oxygens can exist in Sb−O−Sb and Sb−O−P bridges. Different to the o-Sb_2O_3 crystal the number of

secondary bonds of lengths 0.24 nm < r_{SbO} < 0.28 nm in the glass is small. The SbO_4 and PO_4 units are forming chain-like structures for reasons of bond valences of the weak axial bonds of the SbO_4 trigonal bipyramids and the overbonded P−O bonds.

The first neutron and X-ray diffraction peaks of sbp80 show two maxima at 13 nm^{-1} and 20 nm^{-1} that are in the positions of the prominent Bragg reflections of the o-Sb_2O_3 crystal. The first peak is related to distances between stacked layers of corner-connected oxygen triangles such as in the crystal. The medium-range order of sample sbp05 reminds that of vitreous P_2O_5 with a majority of threefold linked PO_4 tetrahedra. The Sb^{3+} form SbO_4 units with mean Sb−O bonds of 0.210 nm. It is assumed that these units also possess sterically active electron pairs.

The SbO_3 pyramids with O−Sb−O angles of 90° can be seen as part of the SbO_6 octahedron of crystalline Sb_2O_5. The Sb^{3+} cation forms three primary bonds to one side of solid angle such as a Sb^{5+} cation would do while anti-bonding states screen the second side from any bonding. Sb_2O_3 is a good network-former oxide better than Sb_2O_5.

This research did not receive any specific grant from funding agencies in the public, commercial or not-for-profit sectors.

CRediT author statement:

Uwe Hoppe: Conceptualization, Investigation, Formal analysis, Writing – Original draft. Andreas Schöps: Resources, Investigation. Alex Hannon: Resources, Investigation, Software. Andrea Barz: Resources, Investigation. Dörte Stachel: Conceptualization, Resources, Writing – Review and Editing.

Literature

[1] C. Svensson, The crystal structure of orthorhombic antimony trioxide, Sb_2O_3, Acta Cryst. B 30 (1974) 458-461.

[2] C. Svensson, Refinement of the crystal structure of cubic antimony trioxide, Sb_2O_3, Acta Cryst. B 31 (1975) 2016-2018.

[3] W.H. Zachariasen, The atomic arrangement in glass, J. Am. Chem. Soc. 54 (1932) 3841-3851.

[4] U. Dehlinger, Z. Kristallogr., Über die Kristallstruktur der Antimonoxyde, 66 (1927) 108-119.

[5] M. Nalin, M. Poulain, M. Poulain, S.J.L. Ribeiro, Y. Messaddeq, Antimony oxide based glasses, J. Non-Cryst. Solids 284 (2001) 110-116.

[6] B. Kinberger, The crystal structure of $SbPO_4$, Acta Chem. Scand. 24 (1970) 320-328.

[7] E.L. Falcão-Filho, C.D. de Araújo, C.A.C. Bosco, G.S. Maciel, L.H. Acioli, Antimony orthophosphate glasses with large nonlinear refractive indices, low two-photon absorption coefficients, and ultrafast response, J. Appl. Phys. 97 (2005) 013505.

[8] M. Nalin, Y. Messaddeq, S.J.L. Ribeiro, M. Poulain, V. Briois, G. Brunklaus, C. Rosenhahn, B.D. Mosel, H. Eckert, Structural organization and thermal properties of the Sb_2O_3-$SbPO_4$ glass system, J. Mater. Chem. 14 (2004) 3398-3405.

[9] D. Stachel, C. Magand, Investigations of binary antimony phosphate glasses, Phosphorus Res. Bull. 19 (2005) 325-330.

[10] B.A. Adair, A.K. Cheetham, Synthesis and Structure of Sb_5PO_{10}, a New Phosphate of Antimony(III), J. Solid State Chem. 155 (2000) 451-454.

[11] C. Magand, Binary antimony phosphate glasses, Diploma thesis, University of Jena, 2003.

[12] U. Hoppe, R. Kranold, D. Stachel, A. Barz, A.C. Hannon, Variation in P-O Bonding in Phosphate Glasses – A Neutron Diffraction Study, Z. Naturforsch. A 55 (2000) 369-380.

[13] U. Hoppe, D. Ilieva, J. Neuefeind, The Structure of Gallium Phosphate Glasses by High-energy X-ray Diffraction, Z. Naturforsch. 57 a (2002) 709-715.

[14] U. Hoppe, D. Stachel, D. Beyer, The Oxygen Coordination of Metal Ions in Phosphate and Silicate Glasses Studied by a Combination of X-ray and Neutron Diffraction, Physica Scripta T 57 (1995) 122-126.

[15] U. Hoppe, R.K. Brow, A.C. Hannon, M. v.Zimmermann, Structure of tin phosphate glasses by neutron and X-ray diffraction, J. Non-Cryst. Solids X 2 (2019) 100017.

[16] U. Hoppe, I. Gugov, H. Bürger, P. Jóvári, A.C. Hannon, Structure of tellurite glasses – effects of K_2O or P_2O_5 additions studied by diffraction, J. Phys.: Condens. Matter 17 (2005) 2365-2386.

[17] D. Waasmaier, A. Kirfel, New analytical scattering-factor functions for free atoms and ions, Acta Cryst. A51 (1995) 416-431.

[18] E.N. Maslen, A.G. Fox, M.A. O'Kiefe, in: A.J.C. Wilson (Ed.), International Tables for Crystallography, vol. C, Kluwer Academic, Dordrecht, 1992, p. 476.

[19] J.H. Hubbell, Wm.J. Veigele, E.A. Briggs, R.T. Brown, D.T. Cromer, R.J. Howerton, Atomic form factors, incoherent scattering functions, and photon scattering cross sections, J. Phys. Chem. Ref. Data 4 (1975) 471-538.

[20] T.E. Faber, J.M. Ziman, A theory of the electrical properties of liquid metals, Philos. Mag. 11 (1965) 153-173.

[21] Y. Waseda, The Structure of Non-Crystalline Materials, McGraw-Hill, New York, 1980, p. 11.

[22] A.C. Hannon, Results on disordered materials from the GEneral Materials diffractometer, GEM, at ISIS, Nucl. Instrum. & Meth. A 551 (2005) 88-107.

[23] U. Hoppe, G. Walter, R. Kranold, D. Stachel, An X-ray Diffraction Study of the Structure of Vitreous P_2O_5, Z. Naturforsch. 53 a (1998) 93-104.

[24] R.L. Mozzi, B.E. Warren, The structure of vitreous silica, J. Appl. Cryst. 2 (1969) 164.

[25] A.J. Leadbetter, A.C. Wright, Diffraction studies of glass structure: I. Theory and quasi-crystalline model, J. Non-Cryst. Solids 7 (1972) 23-36.

[26] A.C. Hannon, Neutron diffraction techniques for structural studies of glasses, in: Modern Glass Characterization, ed. M. Affatigato, John Wiley & Sons, Hoboken, New Jersey, 2015, p 190ff.

[27] M. Jansen, Die Kristallstruktur von Antimon(V)-oxid, Acta Cryst. B 35 (1979) 539-542.

[28] I.D. Brown, D. Altermatt, Bond-valence parameters obtained from a systematic analysis of the inorganic crystal structure database, Acta Cryst. B 41 (1985) 244-247.

[29] S.J. Mills, A.G. Christy, E.C.-C. Chen, M. Raudsepp, Revised values of the bond valence parameters for $^{[6]}$Sb(V)−O and $^{[3-11]}$Sb(III)−O, Z. Kristallogr. 224 (2009) 423-431.

[30] O.C. Gagné, F.C. Hawthorne, Comprehensive derivation of bond-valence parameters for ion pairs involving oxygen, Acta Cryst. B 71 (2015) 562-578.

[31] E.H. Arbib, B. Elouadi, J.P. Chaminade, J. Darriet, New refinement of the crystal structure of o-P_2O_5, J. Solid State Chem. 127 (1996) 350-353.

[32] D. Stachel, I. Svoboda, H. Fuess, Phosphorus Pentoxide at 233 K, Acta Cryst. C 51 (1995) 1049-1050.

[33] K. Meyer, Characterisation of the structure of binary calcium ultraphosphate glasses by infrared and Raman spectroscopy, Phys. Chem. Glasses 39 (1998) 108-117.

[34] H. Mohmoh, M. Ouchetto, M. Couzi, J.P. Chaminade, E. Arbib, B. Elouadi, Structural relationship between vitreous P_2O_5 and its relevant crystalline polymorphs by Raman spectroscopy, Phosphorus Res. Bull. 13 (2002) 187-192.

[35] J.R. van Wazer, Phosphorus and its Compounds, Vol I (Interscience, New York, 1958) p. 717 ff.

[36] U. Hoppe, A structural model for phosphate glasses, J. Non-Cryst. Solids 195 (1996) 138-147.

[37] A. Dietzel, Die Kationenfeldstärken und ihre Beziehungen zu Entglasungsvorgängen, zur Verbindungsbildung und zu den Schmelzpunkten von Silicaten, Z. Elektrochem. 48 (1942) 9-23.

[38] I.D. Brown, View of Lone Electron Pairs and Their Role in Structural Chemistry, J. Phys. Chem. A 115 (2011) 12638-12645.

[39] R.J. Gillespie, R.S. Nyholm, Inorganic stereochemistry, Quart. Rev. Chem. Soc. 11 (1957) 339-380.

[40] L.E. Orgel, 769. The Stereochemistry of B Subgroup Metals. Part II. The Inert Pair, J. Chem. Soc. (1959) 3815-3819.

[41] J.-M. Raulot, G. Baldinozzi, R. Seshadri, P. Cortona, An ab-initio study of the rôle of lone pairs in the structure and insulator–metal transition in SnO and PbO, Solid State Sci. 4 (2002) 467-474.

[42] A. Walsh, D.J. Payne, R.G. Egdell, G.W. Watson, Stereochemistry of post-transition metal oxides: revision of the classical lone pair model, Chem. Soc. Rev. 40 (2011) 4455-4463.

[43] Y. Du, H.-C. Ding, L. Sheng, S.Y. Savrasov, X. Wan, C.-G. Duan, Microscopic origin of stereochemically active lone pair formation from orbital selective external potential calculations, J. Phys.: Cond. Matter 26 (2014) 025503.

[44] A.G. Christy, S.J. Mills, Effect of lone-pair stereoactivity on polyhedral volume and structural flexibility: application to $Te^{IV}O_6$ octahedra, Acta Cryst. B 69 (2013) 446-456.

[45] M.K. Kim, S.-H. Kim, H.-Y. Chang, P.S. Halasyamani, K.M. Ok, New noncentrosymmetric tellurite phosphate material: synthesis, characterisation, and calculations of $Te_2O(PO_4)_2$, Inorg. Chem. 49 (2010) 7028-7034.

[46] M.A.T. Marple, M. Jesuit, I. Hung, Z. Gan, S. Feller, S. Sen, Structure of TeO_2 glass: Results from 2D ^{125}Te NMR spectroscopy, J. Non-Cryst. Solids 513 (2019) 183-190.

[47] Y. Xia, M.A.T. Marple, I. Hung, Z. Gan, S. Sen, Network Structure and Connectivity in $SnO–P_2O_5$ Glasses: Results from 2D ^{31}P and ^{119}Sn NMR Spectroscopy, J. Phys. Chem. B 122 (2018) 7416-7425.

[48] U. Hoppe, R. Kranold, A. Ghosh, C. Landron, J. Neuefeind, P. Jóvári, Environments of lead cations in oxide glasses probed by X-ray diffraction, J. Non-Cryst. Solids 328 (2003) 146-156.

[49] O.L.G. Alderman, A.C. Hannon, D. Holland, R. Dupree, S. Feller, Structural origin of the weak germanate anomaly in lead germanate glass properties, J. Am. Ceram. Soc. (2021) 1-21.

[50] O.L.G. Alderman, A.C. Hannon, D. Holland, S. Feller, G. Lehr, A.J. Vitale et al., Lone-pair distribution and plumbite network formation in high lead silicate glass, $80PbO·20SiO_2$, Phys. Chem. Chem. Phys. 15 (2013) 8506-8519.

[51] D. Le Bellac, J.M. Kiat, P. Garnier, Electronic Lone Pair Localization and Electrostatic Energy Calculations: Application to α-PbO, SnO, $Pb_{1-x}(TiO)_xO$, Pb_3O_4, $Pb_3(V,P)_2O_8$, and a BiSrCaCuO-Type Superconductor, J. Solid State Chem. 114 (1995) 459-468.

Table 1. Weighting factors w_{ij} of the six partial contributions of the total neutron and X-ray correlation functions for the samples measured. The factors of the X-ray data are approximate values based on the electron numbers. The underlines indicate the weighting strength (strong – solid line; medium – dashed line; weak – no line).

Atom pair	sbp05 ND	sbp05 HEXRD	sbp80 ND	sbp80 HEXRD
P–O	0.3694	0.4216	0.0859	0.0248
Sb–O	0.0211	0.0755	0.3731	0.3371
O–O	0.5387	0.2899	0.4137	0.0563
P–P	0.0633	0.1533	0.0045	0.0027
Sb–P	0.0072	0.0549	0.0387	0.0742
Sb–Sb	0.0002	0.0049	0.0841	0.5048

Table 2. Parameters of the Gaussian functions used to model the first-neighbor peaks of the $T_X(r)$ and $T_N(r)$ functions of the $(Sb_2O_3)_x(P_2O_5)_{1-x}$ glasses of x = 0.05 and 0.80 as shown in Fig. 2. The parameters marked with [a] were fixed in the fits. The differences of the two distances that are used to model the P−O peaks were also fixed [b]. The Sb−O distances larger than 0.25 nm and the O−O distances larger than 0.26 nm marked with [c] were adjusted by eye to the $T_N(r)$ and $T_X(r)$ in the range up to 0.30 nm. The distances and fwhm (full width at half height of the maximum) are given in nm.

Sample label	Atom pair	Coordination number	Distance	fwhm
sbp05	P−O	1.47(8)	0.1477[b]	0.013(2)
		2.26(12)	0.1587[b]	0.011(1)
	Sb−O	3.6(2)	0.2065(20)	0.022(5)
		0.5(3)	0.236(5)	0.030(8)
	O−O	4.85(20)	0.252[a]	0.024(3)
sbp80	P−O	2.97(15)	0.154[b]	0.013(2)
		1.28(10)	0.162[b]	0.007(3)
	Sb−O	2.10(10)	0.197(2)	0.013(3)
		0.70	0.210	0.018(5)
		0.50	0.228	0.025(5)
		0.20[c]	0.256[c]	0.025[c]
		0.10[c]	0.270[c]	0.030[c]
		1.10[c]	0.296[c]	0.030[c]
	O−O	1.46(10)	0.252[a]	0.020(3)
		1.25[c]	0.270[c]	0.025[c]
		2.65[c]	0.287[c]	0.035[c]
	Sb−P	1.0[a]	0.33[a]	0.030[a]
	Sb−Sb	2.25[a]	0.35[a]	0.035[a]

Table 3. Total coordination numbers and mean distances of the P−O and Sb−O bonds of the two samples measured as calculated from the parameters in Table 2. The distances are given in nm.

Sample label	Atom pair	Coordination number	Distance
sbp05	P−O	3.73(20)	0.1544(10)
	Sb−O	4.1(4)	0.210(3)
sbp80	P−O	4.25(25)	0.1564(15)
	Sb−O	3.3(2)	0.204(2)

Figure captions

Fig. 1. Neutron and X-ray structure factors by means of the weighted interference function $Q\cdot[S(Q)-1]$ of the glasses $(Sb_2O_3)_x(P_2O_5)_{1-x}$ of x = 0.05 (sbp05) and 0.80 (sbp80). The upper curves are shifted for clarity of the plot.

Fig. 2. Neutron and X-ray correlation functions $T(r)$ of the $(Sb_2O_3)_x(P_2O_5)_{1-x}$ glasses with x = 0.05 (a) and 0.80 (b) as obtained by Fourier transform (Eq. 2) with Q_{max} = 273 nm^{-1} (X-rays) and 450 nm^{-1} (neutrons), both with Lorch damping (Eq. 3). The experimental data (black dots) are compared with model functions (thick red lines). The partial functions of the atom pairs are given with thin lines: P−O (solid), Sb−O (dashed) and O−O (dash-dotted lines). The distance peaks Sb−P (solid) and Sb−Sb (dash-dot-dot lines) are added for sample sbp80 with meaningful but fixed parameters. The distance peaks at ~0.28 nm that belong to the O−O and Sb−O correlations were adjusted by hand (see text). The upper functions are shifted for clarity. (For interpretation of the colors in the figure, the reader is referred to the web version of this article.)

Fig. 3. Section of a network formed of SbO_3 trigonal pyramids. To illustrate the height of the Sb above the base triangle the corresponding distances are given by solid-lined arrows in two of the SbO_3 pyramids. The triangles defined by the O sites are forming a network layer. (For interpretation of the colors in the figure, the reader is referred to the web version of this article.)

Fig. 4. Neutron and X-ray structure factors $S(Q)$ in the low-Q region. The vertical dashed lines indicate the Q-values of the first three Bragg-reflections of the orthorhombic Sb_2O_3 crystal [1]. The upper curves are shifted for clarity.

Fig. 5. Low-Q regions of the neutron and X-ray structure factors $S(Q)$ of the $(Sb_2O_3)_x(P_2O_5)_{1-x}$ glasses of x = 0.05 (a) and 0.80 (b) in comparison with the powder pattern of the related crystal structures where the Bragg-reflections are strongly broadened. Vertical dashed lines mark the positions of the reflections (111) and (240) at 14.7 nm^{-1} and 21.8 nm^{-1} of the o-P_2O_5 crystal [25] and (110), (111), and (121) at 13.8 nm^{-1}, 18.0 nm^{-1}, and 20.0 nm^{-1} of the o-Sb_2O_3 crystal [1]. The upper curves are shifted for clarity.

Fig. 6. Section of a network formed of SbO_3, SbO_4 and PO_4 units. The SbO_4 trigonal bipyramids (via their axial corners) and the PO_4 tetrahedra are forming chain structures. The equatorial corners of the SbO_4 are linked with PO_4 or SbO_3 units. (For interpretation of the colors in the figure, the reader is referred to the web version of this article.)

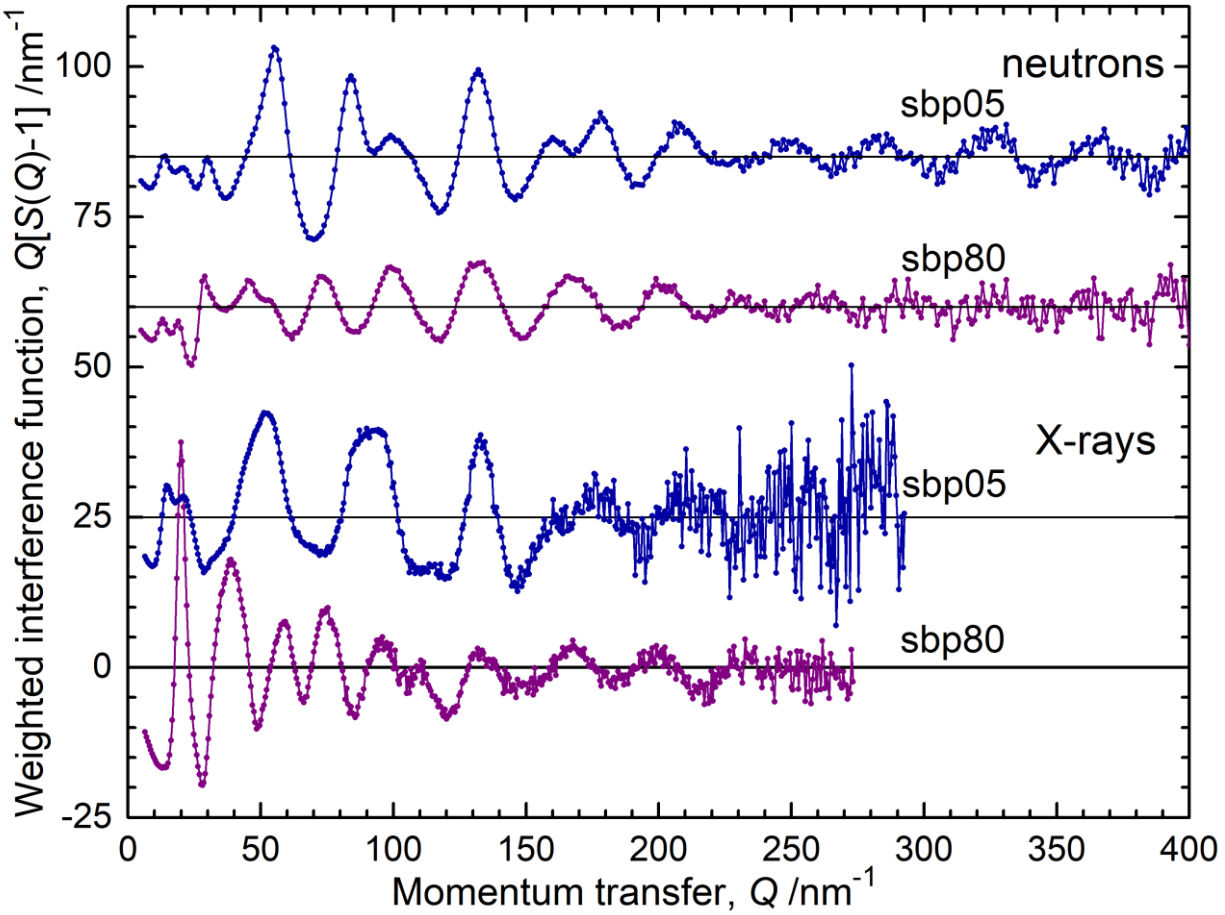

Fig. 1. Neutron and X-ray structure factors by means of the weighted interference function $Q\cdot[S(Q)-1]$ of the glasses $(Sb_2O_3)_x(P_2O_5)_{1-x}$ of x = 0.05 (sbp05) and 0.80 (sbp80). The upper curves are shifted for clarity of the plot.

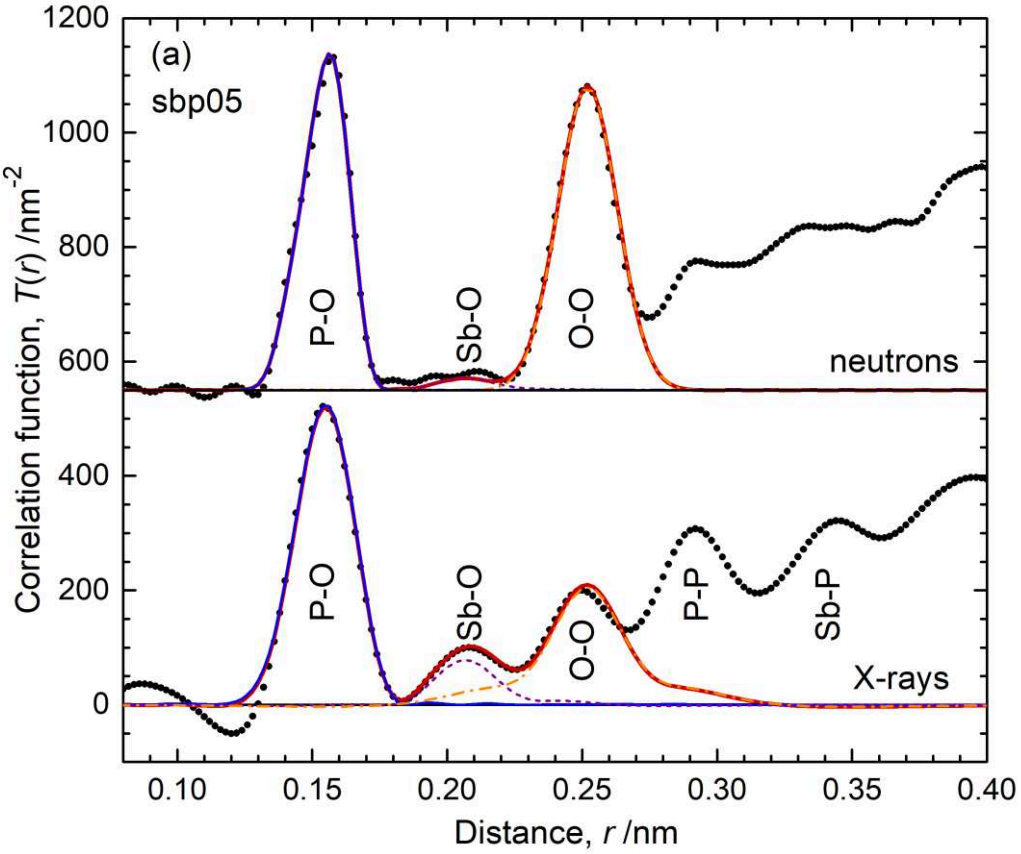

Fig. 2a

Fig. 2. Neutron and X-ray correlation functions $T(r)$ of the $(Sb_2O_3)_x(P_2O_5)_{1-x}$ glasses with $x = 0.05$ (a) and 0.80 (b) as obtained by Fourier transform (Eq. 2) with $Q_{max} = 273$ nm^{-1} (X-rays) and 450 nm^{-1} (neutrons), both with Lorch damping (Eq. 3). The experimental data (black dots) are compared with model functions (thick red lines). The partial functions of the atom pairs are given with thin lines: P−O (solid), Sb−O (dashed) and O−O (dash-dotted lines). The distance peaks Sb−P (solid) and Sb−Sb (dash-dot-dot lines) are added for sample sbp80 with meaningful but fixed parameters. The distance peaks at ~0.28 nm that belong to the O−O and Sb−O correlations were adjusted by hand (see text). The upper functions are shifted for clarity. (For interpretation of the colors in the figure, the reader is referred to the web version of this article.)

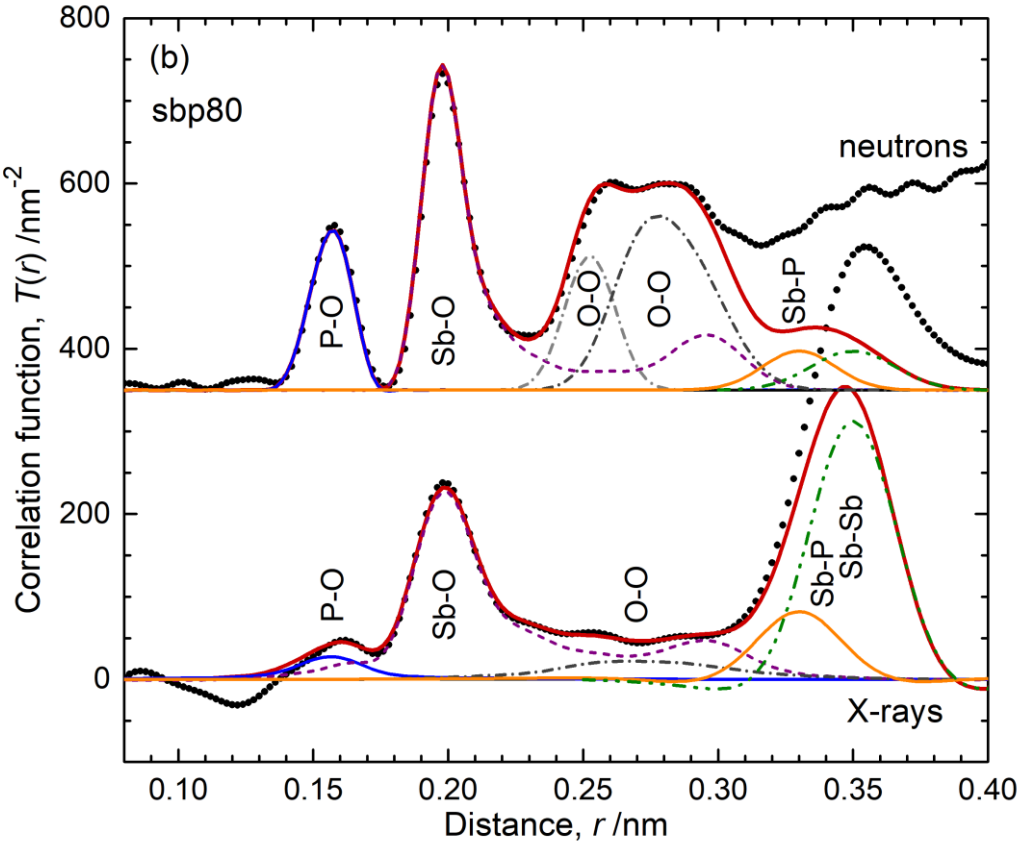
(b)
sbp80
neutrons
X-rays
P-O
Sb-O
O-O
O-O
Sb-P
P-O
Sb-O
O-O
Sb-P
Sb-Sb
Correlation function, T(r) /nm-2
Distance, r /nm
800
600
400
200
0
0.10
0.15
0.20
0.25
0.30
0.35
0.40

Fig. 2b

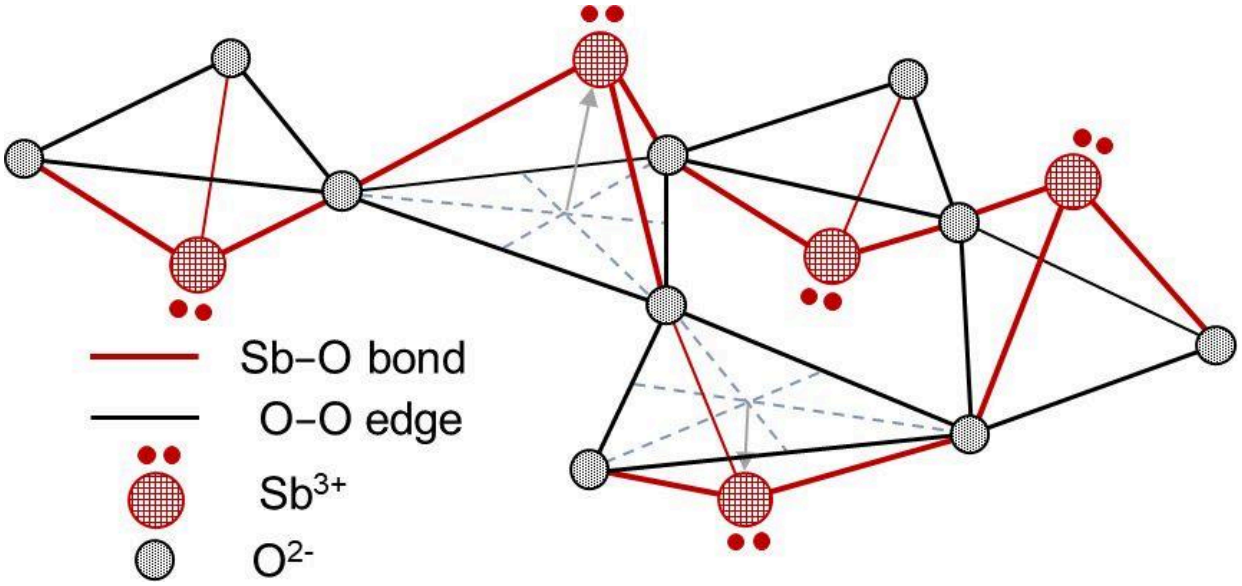

Fig. 3. Section of a network formed of SbO_3 trigonal pyramids. To illustrate the height of the Sb above the base triangle the corresponding distances are given by solid-lined arrows in two of the SbO_3 pyramids. The triangles defined by the O sites are forming a network layer. (For interpretation of the colors in the figure, the reader is referred to the web version of this article.)

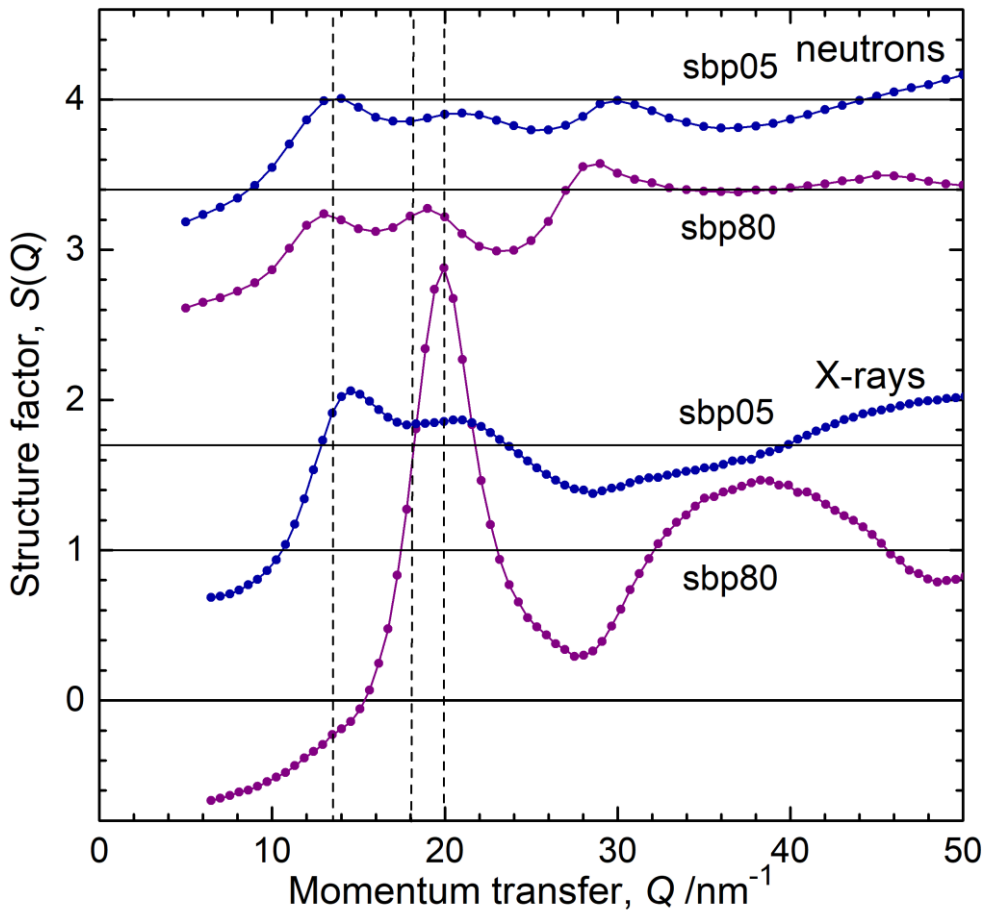

Fig. 4. Neutron and X-ray structure factors $S(Q)$ in the low-Q region. The vertical dashed lines indicate the Q-values of the first three prominent Bragg-reflections of the orthorhombic Sb_2O_3 crystal [1].

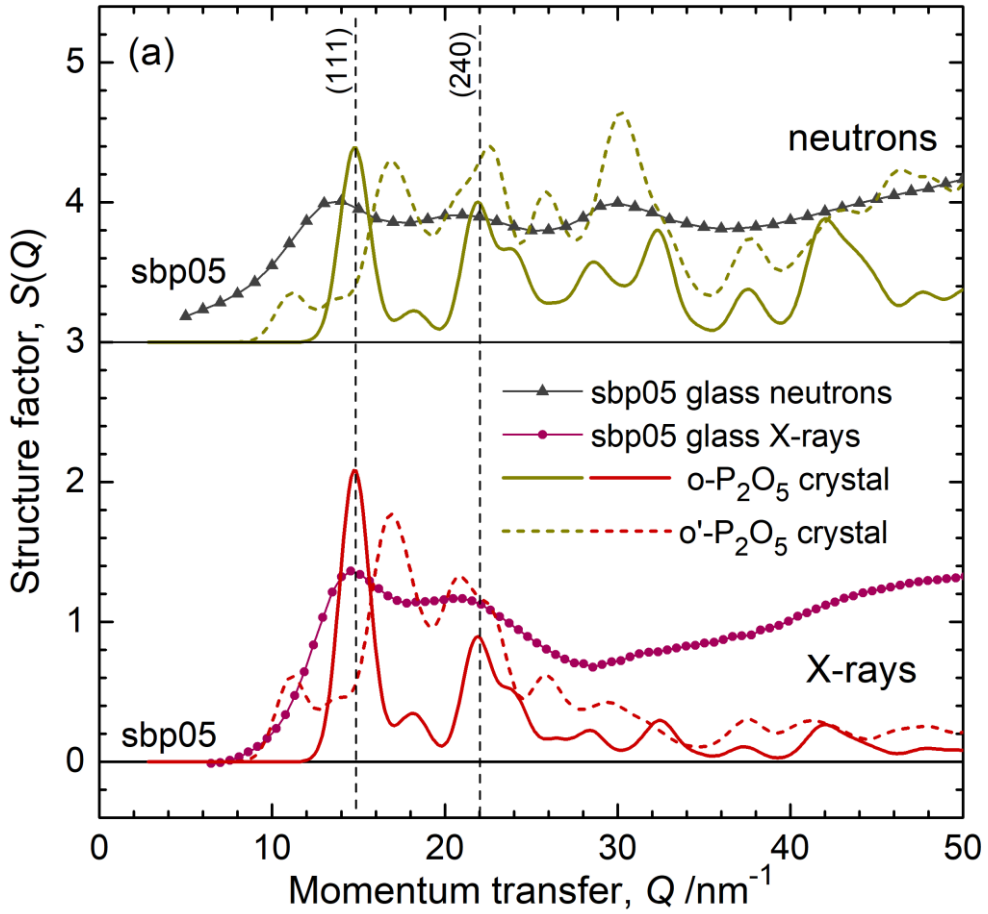

Fig.5a

Fig. 5. Low-*Q* regions of the neutron and X-ray structure factors *S*(*Q*) of the $(Sb_2O_3)_x(P_2O_5)_{1-x}$ glasses of $x = 0.05$ (a) and 0.80 (b) in comparison with the powder pattern of the related crystal structures where the Bragg-reflections are strongly broadened. Vertical dashed lines mark the positions of the reflections (111) and (240) at 14.7 nm^{-1} and 21.8 nm^{-1} of the o-P_2O_5 crystal [25] and (110), (111), and (121) at 13.8 nm^{-1}, 18.0 nm^{-1}, and 20.0 nm^{-1} of the o-Sb_2O_3 crystal [1]. The upper curves are shifted for clarity.

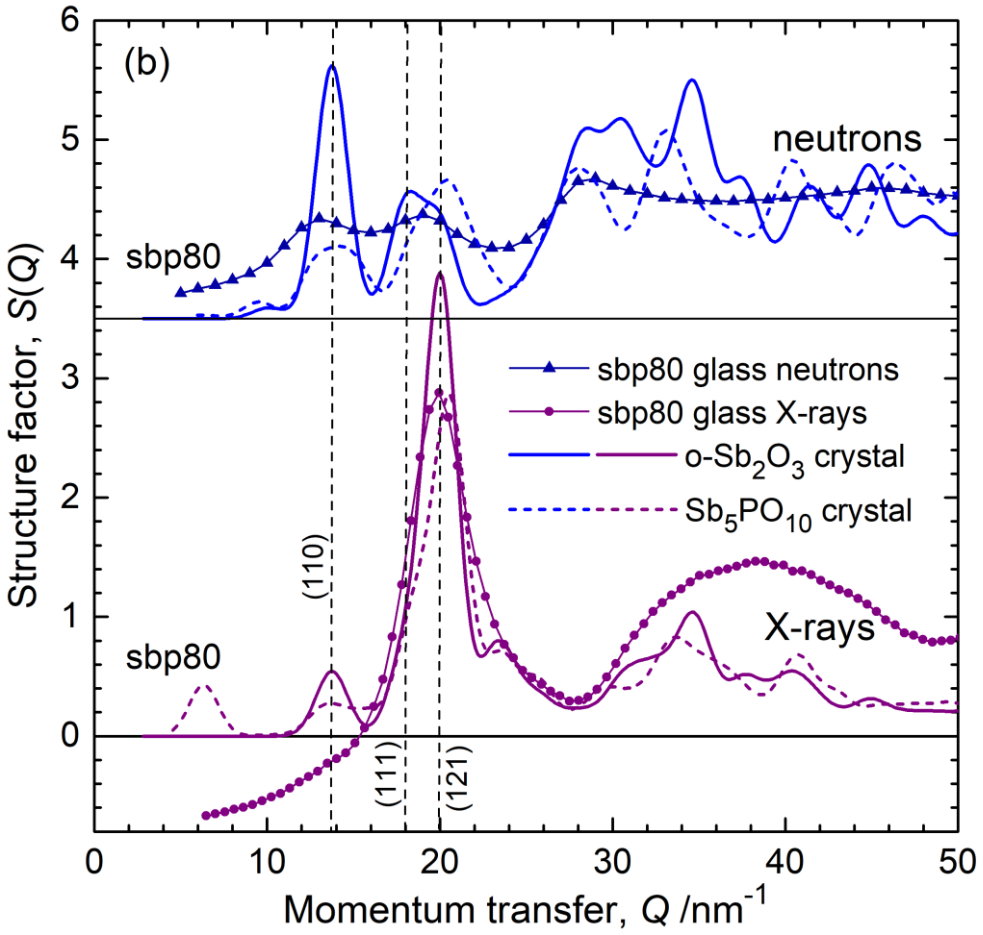
(b)
neutrons
sbp80
sbp80 glass neutrons
sbp80 glass X-rays
o-Sb2O3 crystal
Sb5PO10 crystal
(110)
(111)
(12$\bar{1}$)
X-rays
sbp80
Structure factor, S(Q)
Momentum transfer, Q /nm-1
0
10
20
30
40
50
0
1
2
3
4
5
6

Fig. 5b

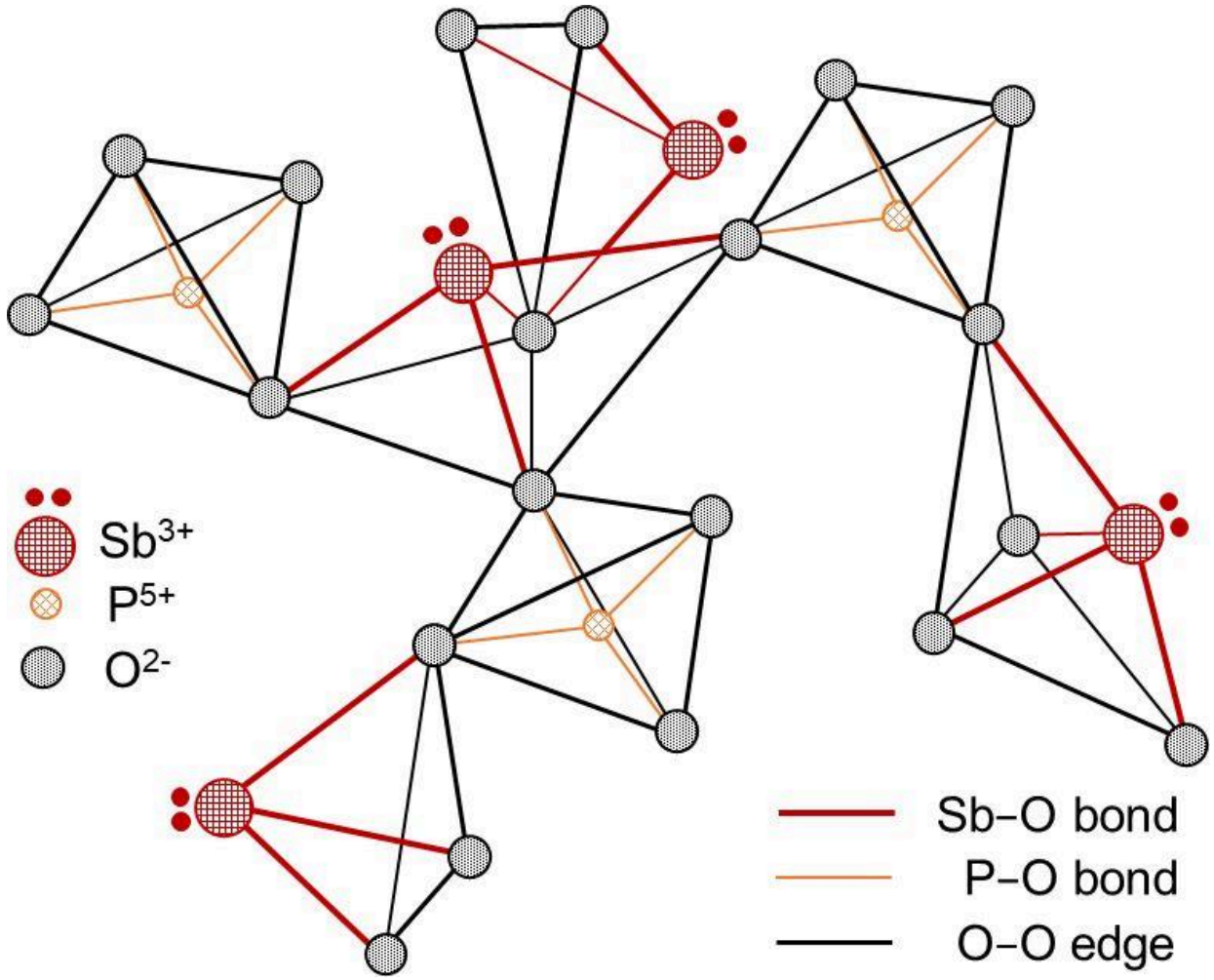

Fig. 6. Section of a network formed of SbO_3, SbO_4 and PO_4 units. The SbO_4 trigonal bipyramids (via their axial corners) and the PO_4 tetrahedra are forming chain structures. The equatorial corners of the SbO_4 are linked with PO_4 or SbO_3 units. (For interpretation of the colors in the figure, the reader is referred to the web version of this article.)

Declaration of interests

☒The authors declare that they have no known competing financial interests or personal relationships that could have appeared to influence the work reported in this paper.

☐The authors declare the following financial interests/personal relationships which may be considered as potential competing interests:

on behalf of all contributing authors

Uwe Hoppe